Pergamon

0956-7151(94)E0162-A

Acta metall. mater. Vol. 42, No. 11, pp. 3801–3809, 1994
Copyright © 1994 Elsevier Science Ltd
Printed in Great Britain. All rights reserved
0956-7151/94 $7.00 + 0.00

INTERNAL FRICTION IN F.C.C. ALLOYS DUE TO SOLUTE DRAG ON DISLOCATION—II. EXPERIMENTAL STUDIES ON Al–Si ALLOYS

A. PICHLER,† M. WELLER and E. ARZT

Max-Planck-Institut für Metallforschung and Institut für Metallkunde der Universität Stuttgart, D-70174 Stuttgart, Germany

(Received 16 July 1993; in revised form 23 February 1994)

Abstract—Internal friction (mechanical loss) experiments were carried out on single crystal and polycrystalline Al–Si alloys with incoherent Si particles of varying size, spacing, and as a function of pre-strain. The resulting internal friction spectra are correlated with microstructural investigations. The loss maximum at about 450 K ($f \sim 1$ Hz), especially its "low" activation enthalpy of $H = 1.14$ eV, can be explained by our dislocation model described in the companion paper (Part I), which considers the enhanced transverse diffusivity of solute atoms in the vicinity of the dislocation core. The model is also shown to be in agreement with published data on Al–Si, Al–Mg, Cu–Si and Cu–Al. It is proposed that in many instances the internal friction maxima, even when characterized by a "low" activation enthalpy, need not be due to grain boundary or particle effects, but may well be explained by core diffusion effects on solute drag acting on dislocations.

1. INTRODUCTION

Many aluminium alloys with incoherent particles exhibit, regardless of their composition, internal friction (mechanical loss) maxima at temperatures between 400 and 500 K at about 1 Hz [1–6]. For explaining the maxima, different mechanisms are proposed and discussed in the literature. Most authors invoke a grain boundary mechanism, in which the particles reduce the sliding distance between the triple nodes and therefore lower the temperature of the grain boundary maximum [4, 6–8]. The other mechanism [9, 10] is the relaxation of stress in the particles by diffusion in the particle–matrix interface.

Some authors report conflicting evidence from which it is not clear which mechanistic interpretation should be favored. For example, Okabe *et al.* [10] carried out internal friction measurements on both single crystal and polycrystalline Al samples with incoherent Si particles of different sizes and found similar maxima in both types of specimens. They obtained good agreement between the experimental results and the model of Mori *et al.* [9]. By contrast, Entwistle *et al.* [11] found the maximum only in polycrystalline samples of similar Al–Si alloys and attributed it to grain boundary sliding. An alternative explanation, which was not considered in either investigation, lies in the possible role of dislocations. For f.c.c. metals containing impurities, mechanisms in which the kinetics of the dislocation motion is determined by the concurrent movement of a Cottrell cloud, e.g. as in the model of Schoeck [12, 13], have not been invoked for explaining experiments in the past.

In this paper new internal friction experiments on Al–Si alloys with incoherent Si particles are reported. To illuminate the possible influences of dislocations, grain boundaries, particles, and the interaction between these defects, samples with different microstructures, i.e. grain size, particle size, and dislocation density and arrangement, were produced and investigated. In particular, the behavior of single crystals was compared with that of polycrystals. From a correlation between the different internal friction spectra and the microstructure, as investigated by TEM, conclusions on the mechanisms are drawn. The experimental results are discussed in the light of our recent dislocation model [14], in which the enhanced diffusion of the solute atoms in the dislocation core is considered. It is also shown that the contradiction between the results of Okabe *et al.* and Entwistle *et al.* may thus be resolved and that other experimental results on Al and Cu alloys can be explained in a natural way.

2. EXPERIMENTAL

2.1. Preparation and characterization of the Al–Si alloy

Sample preparation started from 5N Al (Cu ~ 0.6 ppm, Mg ~ 0.7 ppm, Si ~ 1 ppm) and 6N Si, which were molten and cast in an Al_2O_3 crucible under Ar. The castings were swaged from a diameter of 10 to

†Present address: VOEST ALPINE Stahl Linz GmbH, Linz, Austria.

Table 1. The Al–Si specimens investigated

Sample	f_V (%)	T (K)	t (h)	a (nm)	l_p (nm)	φ
S1	0.72	553	10	53	452	Handling
S2	0.60	573	10	64	598	Handling
S3	0.54	593	10	73	720	Handling
SD	0.69	573	10	62	540	0.15
P	0.52	573	10	58	582	Handling

f_V—volume fraction of the Si precipitations, T—aging temperature, t—aging time, a—particle size, l_p—mean planar particle distance, and φ—deformation

4.5 mm. A recrystallization treatment at $T = 520°C$ for 3 min resulted in a grain size of 0.1 mm. Single crystals were produced with the strain-anneal method [15], involving a critical straining of 1.2% and a travelling velocity of 1 cm/h to a hot (853 K) salt bath. In order to obtain different particle distributions, samples were aged at various temperatures for 10 h. The parameters and the nomenclature of the samples are listed in Table 1. The Si content was determined by wet chemistry, and the volume fraction of Si particles was calculated under the assumption that Si is insoluble in Al. From the volume fraction f_V and the mean particle size a, the mean planar particle distance $l_p = a \cdot (\pi/6 \cdot f_V)^{0.5}$ was obtained (Table 1). To investigate the influence of deformation, a single crystal (SD) was deformed to about 15% by rolling. Samples with dimensions $4 \times 1 \times 50\,mm^3$ were prepared by spark cutting for the internal friction measurements.

The microstructure was mainly investigated with a JEOL 200CX TEM. After grinding to 100 μm, the samples were thinned at $T = 243$ K and at a voltage of 30–35 V with an electrolyte containing one part HNO_3 and two parts CH_3OH. The size of the Si precipitates was determined from bright field images with the semi-automatic image analyzer "Videoplan". Weak beam images were produced for the study of dislocation structures. The grain size of the polycrystalline sample P was measured in the light microscope by the mean-intercept method, after an etching treatment following Barker [16].

2.2. *Internal friction measurements*

Internal friction (mechanical loss) measurements were carried out with an automatic computer-controlled inverted torsion pendulum [17]. Two types of experiments were performed with this equipment: (i) In the pendulum arrangement different inertias, corresponding to frequencies between 1 and 15 Hz, were used. The internal friction was determined from the logarithmic decrement, δ, of the freely decaying torsional oscillations according to $Q^{-1} = \delta/\pi\,(1 - \delta/2\pi)$. The measurements were performed with increasing temperature, with a mean heating rate of about 2 K/min. The maximum shear strain at the surface was between 1 and 12×10^{-5}. (ii) In another arrangement [18], in which the inertia parts of the pendulum are removed, the loss angle $\varphi h \simeq Q^{-1}$—i.e. the angle between applied stress and resulting strain—was measured for forced vibrations at constant temperature by variation of the applied frequency f ($f = \omega/2\pi$) between 10^{-4} and 40 Hz. The accuracy of φ was estimated from repeated measurements as $\Delta\varphi = \pm 2 \div 5 \times 10^{-4}$ rad. The temperature drift during one $Q^{-1}(\omega)$ measurements (extending over 8–12 h) was smaller than 1 K. For all experiments a static pressure of 1 mbar He was maintained inside the pendulum.

The measured loss spectra were decomposed by fitting with Debye maxima including a log-normal distribution of relaxation times [19]. For the $Q^{-1}(T)$ measurements we subtracted a background (increasing with temperature) consisting of a superposition of a linear and exponential term. For the $Q^{-1}(\omega)$ measurements different backgrounds were subtracted at high and low frequencies. The low frequency part was fitted by a simple approximation corresponding to the tail of a Debye maximum with a log-normal distribution, $Q_{BL}^{-1} = A/\omega^B$, where A and B are fit parameters. The high frequency background, resulting mainly from the mechanical parts of the equipment, was fitted by $Q_{BH}^{-1} = C \cdot \omega + D \cdot \tan(\varphi) \cdot \omega^2$, where C and D are fit parameters [20].

From the displacement of the temperature T_p at the maximum (measurements with variable temperature) and the frequency $\omega_p/2\pi$ at the maximum (measurements with variable frequency), the activation enthalpy H and the inverse attempt frequency τ_0 of the relaxation process were calculated according to

$$\omega_p \cdot \tau_p = 1 = \omega_p \cdot \tau_0 \cdot \exp(H/kT_p). \qquad (1)$$

3. RESULTS

3.1. *Microstructure*

Figure 1 shows a typical microstructure of a single crystal (S2). The dislocation density is for a single crystal surprisingly high, which may be explained by deformation during spark machining. It is remarkable that most of the dislocations are in contact with the particles, which act as firm pinning points. For the deformed single crystal (SD), it is difficult to visualize a representative microstructure as during the first measurement serious alterations take place.

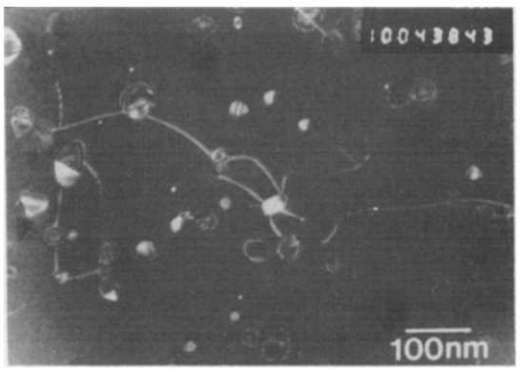

Fig. 1. TEM micrograph of single crystal S2 showing the arrangement of the Si particles and the dislocation structure. (Specimens S1 and S3 have similar microstructure.)

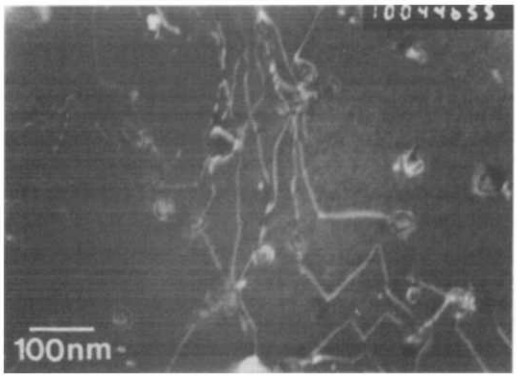

Fig. 2. TEM micrograph showing the dislocation structure in a rolled (strain $\varphi = 15\%$) single crystal (SD) after thermal treatment at 450 K for 10 min.

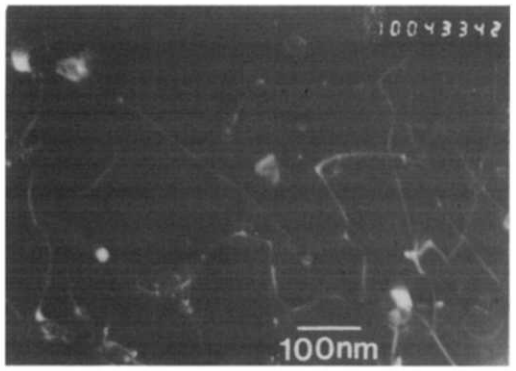

Fig. 5. TEM micrograph of the dislocation structure in the polycrystalline sample P.

To simulate the microstructure which is expected at the maximum temperature of the first run, a sample was annealed at 450 K for 10 min after deformation. In such a pre-treated single crystal the dislocation density is higher than in the as-grown state by about a factor of 5 (Fig. 2). In some regions the dislocations are arranged in irregular networks. For producing a microstructure typical of the second run of the internal friction measurements, a sample was annealed at 540 K for 2 h after deformation. During this treatment the dislocation density decreased significantly (Fig. 3). In particular, the appearance of nearly perfect dislocation networks is observed pointing to strong recovery.

The grain size in the polycrystalline material P is 0.1 mm (Fig. 4). The arrangement of the dislocations is similar as in S2; only the dislocation density is 2–5 times higher (Fig. 5).

3.2. *Internal friction spectra*

As shown in Fig. 6, a loss maximum was detected in the polycrystalline sample P and a single crystal (S2) at nearly the same temperature, but the relaxation strength in P is 5 times higher than in the single crystal. The deformed single crystal (SD) shows a higher maximum at a lower temperature with a more pronounced background. In a second measurement of the same sample, the height of the maximum decreased by about 80%, whereas the background remained unchanged. Additional measurements did not produce further changes in the spectrum.

To investigate the influence of different particle distributions, experiments were conducted on single crystals which had been subjected to different aging treatments (Table 1). For coarser particles (larger particle sizes and mean planar particle distances), the

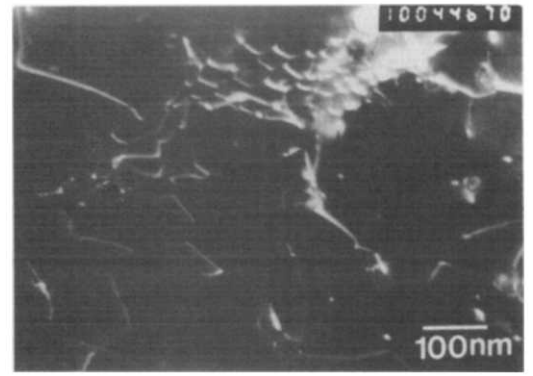

Fig. 3. As in Fig. 2 after thermal treatment at 540 K for 2 h.

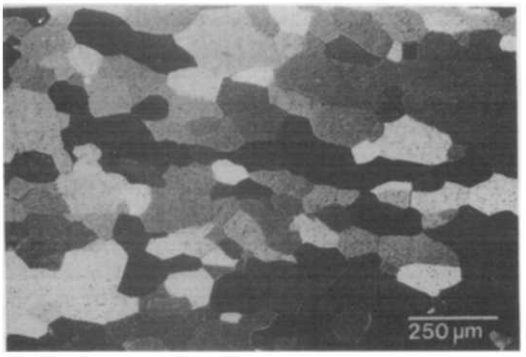

Fig. 4. Light micrograph of the grain structure in sample P, etched according to Barker [16].

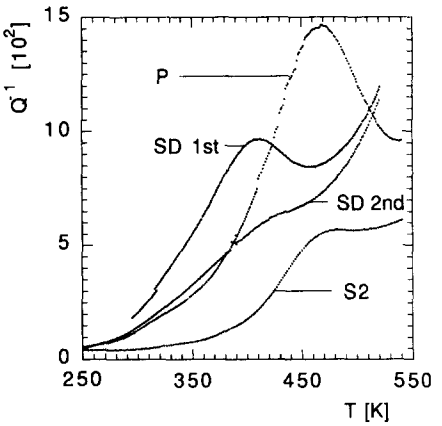

Fig. 6. Internal friction spectra $Q^{-1}(T)$ for the polycrystalline sample (P), an undeformed single crystal (S2) and a deformed single crystal (SD). Measurement frequency about 3.5 Hz.

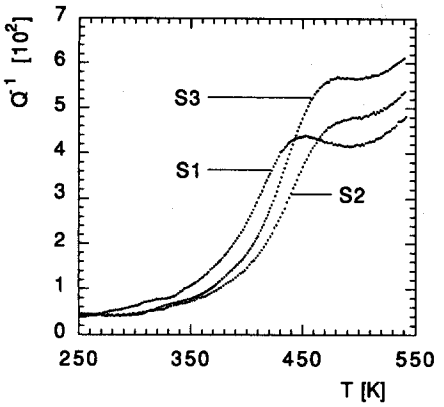

Fig. 7. Internal friction spectra for three single crystals with increasing particle sizes and spacings (S1 → S2 → S3). The temperatures at the maximum are 458 K (S1), 463 K (S2) and 470 K (S3).

Table 2. The activation enthalpy H and the inverse attempt frequency τ_0 for the single crystal S2 and the polycrystalline sample

		τ_0 (s)	H (eV)
S2	T variation	1.6×10^{-15}	1.23
P	T variation	2.4×10^{-14}	1.14
	f variation	2.9×10^{-15}	1.16

maximum shifts to higher temperatures (Fig. 7) while the relaxation strength does not change significantly.

Values of the activation enthalpy H and the inverse attempt frequency τ_0 are listed in Table 2. For the polycrystalline sample, the activation enthalpy was determined from measurements with different frequencies $Q^{-1}(f)$ and temperatures $Q^{-1}(T)$ (Fig. 8). For fitting the $Q^{-1}(T)$ measurements the observed asymmetry of the maximum was taken into account by superimposing a small maximum at the low temperature end (Fig. 9). For the single crystal the activation enthalpy was determined only from $Q^{-1}(T)$ measurements.

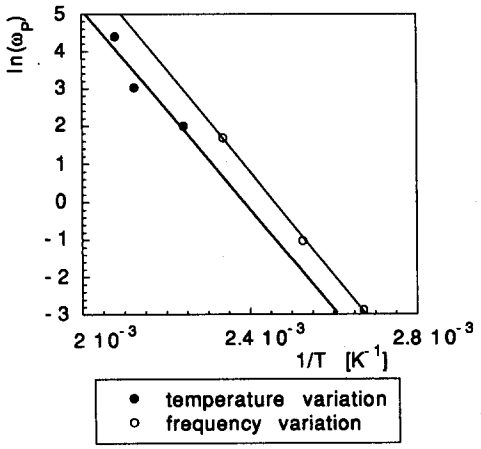

Fig. 8. Arrhenius plots for the internal friction maxima ($\ln \omega_p$ vs $1/T$) obtained for $Q^{-1}(T)$ and $Q^{-1}(\omega)$ measurements (ω_p and T_p denote the angular frequency and the temperature at the maximum, resp.).

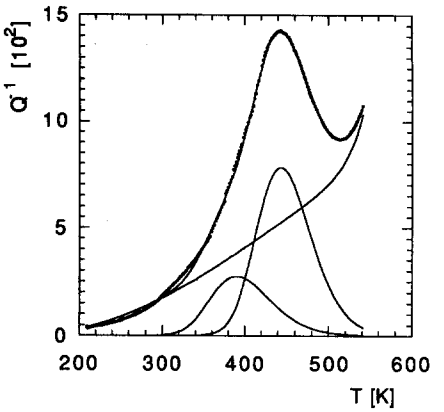

Fig. 9. Decomposition of the internal friction spectrum of the polycrystalline sample P. The smaller maximum at lower temperatures compensates the asymmetry of the maximum.

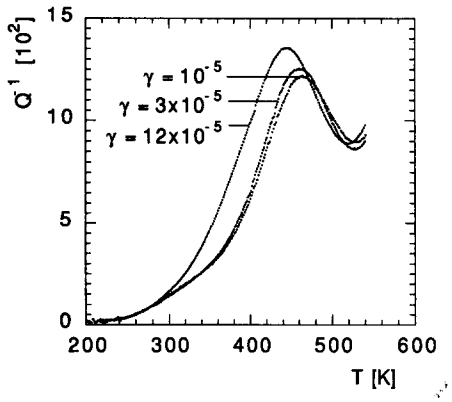

Fig. 10. Internal friction spectra $Q^{-1}(T)$ for the polycrystalline specimen P for three different shear amplitudes.

The internal friction in specimen P was measured for various shear strain amplitudes γ (Fig. 10). For increasing amplitudes the maximum shifts from 463 K ($\gamma = 10^{-5}$) to 444 K ($\gamma = 12 \times 10^{-5}$) and the relaxation strength increases by about 20%. From this shift, the activation volume v_{ex} was estimated using $\tau = \tau_0 \cdot \exp[(H - \sigma_{xy} \cdot v_{ex})/kT)]$, where σ_{xy} is the shear stress $\sigma_{xy} = G \cdot \gamma$ and G the shear modulus. The experimental data can be well fitted with $v_{ex} = 180 \cdot b^3$.

4. DISCUSSION

4.1. Possible mechanisms for internal friction

According to the literature the maximum at 450 K (for a testing frequency of about 3.5 Hz) can be attributed to (i) grain boundary sliding [7, 21, 22], (ii) relaxation of stresses in the particles [9] or (iii) dislocation mechanisms [13, 23–25]. In our experiments the first two may be ruled out for the following reasons: a grain boundary mechanism (i) cannot produce a similar maximum in both the single crystal and the polycrystalline sample, let alone with the same relaxation parameters. For mechanism (ii) the relaxation strength should scale linearly with the volume

fraction of the particles and be independent of grain size [9]. This is in contradiction with the different relaxation strengths in the single crystal and the polycrystalline sample (Fig. 6), both of which contained nearly identical volume fractions of particles. In addition, this mechanism is in conflict with the experimentally observed strong dependence of the maximum on prior deformation and recovery.

This leaves only a dislocation mechanism as an alternative explanation. Which dislocation mechanism can be reconciled with the experimental facts, in particular with the low activation enthalpy, can be narrowed down by model calculations. We therefore discuss the role of the solute atoms for the kinetics of dislocation movement. First it is shown that break-away of the dislocation from its solute cloud is unlikely. Consider a dislocation, which is pinned at distances l and bows out under an external stress *without taking the Cottrell cloud with it* [26]. The resulting energy change U comprises the work done by the external stress (E_σ), the lengthening of the dislocation line (E_L), and the change in the interaction energy between the dislocation and the solute atoms (ΔE_S)

$$U = \Delta E_S + E_L + E_\sigma. \tag{2}$$

These terms are calculated as a function of the bowing-out distance x_d under similar assumptions as in Part I [14]:

(i) For the interaction energy between dislocation and solute atoms the elastic solution for a misfitting sphere in a hydrostatic stress field of a Peierls–Nabarro edge dislocation [14, 27, 28] is applied. The solute concentration around the dislocation at $x, y = 0$ is calculated with the Fermi–Dirac distribution [29]. The change in the interaction energy ΔE_S for a bowing-out distance x_d is given by the difference between the interaction energy for the bowed and the unbowed configuration.

(ii) To calculate the contribution from the lengthening of the dislocation line, the line tension is taken as $Gb^2/2$, where G is the shear modulus and b the Burgers vector. If the bowed-out configuration is described by a circular arc, the energy can be estimated from simple geometrical considerations as

$$E_L = \frac{4}{3} \cdot \frac{G \cdot b^2}{l} \cdot x_d^2. \tag{3}$$

(iii) The energy contribution due to the external stress is estimated as

$$E_\sigma = -G \cdot \gamma \cdot b \cdot l \cdot x_d/2. \tag{4}$$

Table 3. Material data for Al–Si

ϵ	-0.045	[35]
b (nm)	0.286	[27]
ξ (nm)	0.1	[27]
G (GPa)	26.5	[27]
ν	0.347	[27]
Ω (m^3)	1.66×10^{-29}	[27]
D_B (m$\cdot$s^{-2})	$1.7 \times 10^{-4} \cdot \exp(-142000/RT)$	[39]
D_C (m$\cdot$s^{-2})	$1.7 \times 10^{-4} \cdot \exp(-82000/RT)$	[39]

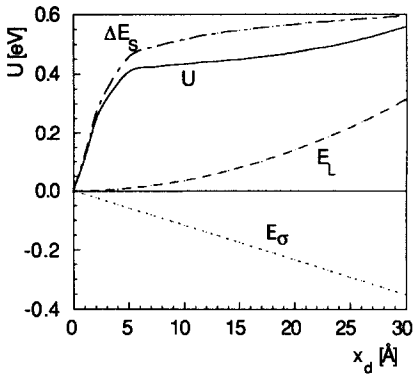

Fig. 11. The energy increment U of a dislocation as function of the bowing-out distance x_d, calculated under the assumption of a fixed solute cloud. E_L is the contribution from the line energy, E_σ the external stress and ΔE_S from the Cottrell cloud.

The calculations of U in equation (2) were performed with the material data for Al–Si as listed in Table 3 and for $\sigma_{xy} = 10^{-5} \cdot G$, $l = 500$ nm, and $T = 400$ K. As discussed in Appendix A1, a reasonable (lower) estimate for the solute concentration corresponding to the solubility limit of Si at $T = 450$ K, is $c_0 \approx 5 \times 10^{-5}$.

The results of these calculations are plotted in Fig. 11 as a function of x_d. It is seen that the energy U of the bowed configuration is always higher than for the unbowed situation; the straight dislocation is, even under external stress, the stable configuration provided that the solute atoms do not move. Calculations with a variation of the parameter c_0 show that this statement holds for solute concentrations larger than 10^{-5}. Thus, the dislocation can bow out *only if the solute atoms diffuse with it* and it is probable that this diffusion mechanism determines the kinetics of the dislocation movement. Such motion can be described by models of Winkler–Gniewek [30, 31], Schoeck [13], and Seeger [32, 33].

Next we examine whether longitudinal movement of the solute, i.e. along the dislocation, or transverse movement, i.e. normal to the dislocation, is expected to dominate. The longitudinal movement of the solute near the dislocation may be favored as the measured activation enthalpy for this process is smaller than that for bulk diffusion; but for this effect to override the uniform distribution along the line, the equation

$$\frac{\gamma^2 \cdot G^2 \cdot b^2 \cdot l^3}{32 \cdot kT \cdot T_L} > 2.35 \cdot n \tag{5}$$

must be fulfilled according to Winkler-Gniewek [30], where T_L is the line tension ($T_L \sim Gb^2/2$) and n the number of solute atoms in the dislocation core of length l. The concentration in the dislocation core is calculated from

$$c = c_0 \cdot \exp(U_B/kT) \tag{6}$$

where U_B is the binding energy between the Si solute atoms and the dislocation, estimated as 0.2 eV [14].

For $\sigma_{xy} = 10^{-5} \cdot G$, $T = 450$ K, $l = 500$ nm and the material data in Table 3 the left-hand side of equation (5) is an order of magnitude lower than the right-hand side and longitudinal diffusion of the solute may thus be excluded.

4.2. Comparison with our solute drag model [14]

Following the arguments of the previous section, we can hypothesize on strong grounds that, under our experimental conditions, the Cottrell clouds move with the dislocations by a mechanism involving transverse diffusion. Several earlier models for such a mechanism exist, especially those of Schoek [13], which treats the dislocation as a string, and of Seeger [32, 33], who takes the kink structure of the dislocations in bcc metals into account. A discrepancy, however, which remains unsolved is the low measured activation enthalpy.

We have developed a model which considers the consequences of a higher solute mobility near the dislocation core [14]: At low solute concentrations c_0 and high strains γ, the kinetics of the dislocation motion is determined by fast diffusion of the solute atoms in the core, while for high c_0 and low γ the diffusion of the solute far away from the dislocation is rate-limiting. Through calculations carried out for Al–Si, a map was constructed which delineates the parameter region where fast diffusion of the solute atoms in the dislocation core determines the relaxation process (Fig. 12). Also shown is the region investigated in our experiments, for which relaxation by solute diffusion in the core region ("core relaxation") is concluded to dominate.

Several predictions of this model are in encouraging agreement with our experimental results. First, the activation enthalpy calculated for this mechanism ($H_m = 1.02$ eV) corresponds reasonably well with the experiments ($H = 1.16$ eV, see Table 2). [Differences in the inverse attempt frequency ($\tau_{0m} = 3.7 \times 10^{-17}$ s and $\tau_{0ex} = 2.9 \times 10^{-15}$ s) should not be over-rated as the local processes in the dislocation core cannot be simulated with the model.]

Secondly, dislocation effects provide a natural explanation for the pre-straining and grain size effects visible in Fig. 6. For dislocation models of this type, the relaxation strength is always given by [13]

$$\Delta \sim \frac{\rho \cdot l^2}{10} \tag{7}$$

where ρ is the dislocation density and l the loop length between the pinning points. The increased internal friction after rolling (first run of SD in Fig. 6) may therefore be ascribed to the higher dislocation density, whereas the lower internal friction in the second run reflects recovery during the first measurement. Also the higher relaxation strength in the polycrystalline sample compared to the single crystal S2 (Fig. 6) can be attributed to the higher dislocation density (compare Figs 1 and 5 for representative TEM images).

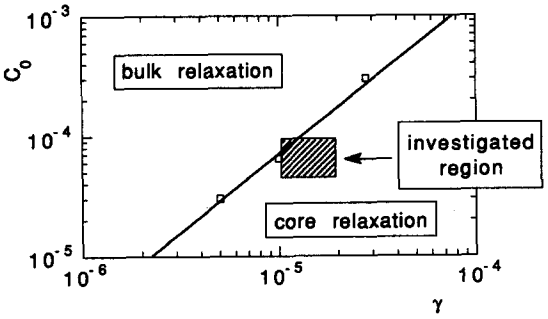

Fig. 12. Map for dominant internal friction processes as a function of the external strain γ and the solute concentration c_0 for Al–Si (from [14]). The experimentally investigated region is shown as the rectangle.

Further, for parameters where the solute in the dislocation core determines the kinetics an analytical expression for the relaxation time is given by equation (12) in [14]

$$\tau = \frac{l^2}{5 \cdot Gb^2} \cdot \frac{kT}{D} \cdot \frac{c_0}{b} \cdot \exp(U_B/kT). \tag{8}$$

Because of the l-dependence, the relaxation time should be sensitive to the arrangement of the dislocations. The shift of the maximum to lower temperatures after deformation (specimen SD) may thus be explained by a shortening of the pinning length, possibly due to nodes produced by dislocation cutting processes.

Third, also the increasing relaxation strengths with increasing external stresses are in agreement with the model (Fig. 8 in [14]). Under a higher stress, the influence of the back stress exerted by the immobile solute atoms far away from the dislocation core is smaller and the dislocation can bow out more strongly.

Fourth, the activation volume may be estimated for the proposed mechanism as

$$v_m = \Delta l \cdot b^2 \tag{9}$$

where Δl is the mean distance between the solute atoms in the dislocation core. For $T = 450$ K, $U_B = 0.2$ eV and $c_0 = 5 \times 10^{-5}$ we obtain $v_m = 116 \cdot b^3$, which is of the same order of magnitude as the experimental value ($v_{ex} = 180 \cdot b^3$).

Finally, the dependence of the temperature at the maximum on the particle distance is a further test for the proposed mechanism. The condition for the maximum $\omega_p \cdot \tau_p = 1$ gives, with equation (8)

$$1 = \omega_p \cdot \tau_p \sim \omega_p \cdot T_p \cdot l^2 \cdot \exp(H/kT_p).$$

(The subscripts p refer to values at the maximum.) Because the mean dislocation length between the pinning points is proportional to the mean planar particle distance, this equation can be written as

$$\ln(\omega_p \cdot T_p) + H/kT_p = -\text{const} - 2\ln(l_p). \tag{10}$$

If the left hand side is plotted against $\ln(l_p)$, a linear relation with a slope of $n = 2$ is expected. Such a